Exploring the initial stages in heavy-ion collisions with high-$p_\perp$ theory and data

Dusan Zigic,[1] Bojana Ilic ⬤,[1] Marko Djordjevic ⬤,[2] and Magdalena Djordjevic ⬤[1,*]

[1]*Institute of Physics Belgrade, University of Belgrade, 11080 Belgrade, Serbia*
[2]*Faculty of Biology, University of Belgrade, 11000 Belgrade, Serbia*

Traditionally, the low-$p_\perp$ sector is used to infer the features of initial stages before quark-gluon plasma thermalization. On the other hand, a recently acquired wealth of high-$p_\perp$ experimental data paves the way to utilize the high-$p_\perp$ particles' energy loss in exploring the initial stages. We here study how four different commonly considered initial-stage scenarios—which have the same temperature profile after thermalization, but differ in the "temperature" profile before thermalization—affect predictions of high-$p_\perp$ R_{AA} and v_2 observables. Contrary to common expectations, we obtain that high-$p_\perp$ v_2 is insensitive to the initial stages of medium evolution, being unable to discriminate between different conditions. On the other hand, R_{AA} is sensitive to these conditions; however, within the current error bars, the sensitivity is not sufficient to distinguish between different initial stages. Moreover, we also reconsider the validity of the widely used procedure of fitting the energy loss parameters, individually for different initial-stage cases, to reproduce the experimentally observed R_{AA}. We here find that previously reported sensitivity of v_2 to different initial states is mainly a consequence of the R_{AA} fitting procedure, which may lead to incorrect conclusions. On the other hand, if a global property, in particular the same average temperature, is imposed to tested temperature profiles, high sensitivity of high-$p_\perp$ v_2 is again obtained. We show, however, that this sensitivity would be a consequence of differences not in initial stages but rather in final stages. Consequently, the simultaneous study of high-$p_\perp$ R_{AA} and v_2, with consistent energy loss parametrization and stringently controlled temperature profiles, is necessary to assess sensitivity of different variables to differences in initial and final stages.

I. INTRODUCTION

It is by now firmly confirmed that a new state of matter— the quark-gluon plasma (QGP) [1,2], in which quarks, antiquarks and gluons are deconfined—is formed at the Relativistic Heavy Ion Collider (RHIC) and the Large Hadron Collider (LHC). Rare high transverse momentum (high-$p_\perp$) particles, which are created immediately upon collision, are sensitive to all stages of QGP evolution, and are considered to be excellent probes [3–6] of this extreme form of matter. As these probes traverse the QGP, they lose energy, which is commonly assessed through high-$p_\perp$ angular averaged (R_{AA}) [7–14] and high-$p_\perp$ angular differential (v_2) [15–19] nuclear modification factors.

Commonly, high-$p_\perp$ particles are used to study the nature of jet-medium interactions, while low-$p_\perp$ particles are used to infer the bulk QGP properties. Accordingly, the scarce knowledge of the features of initial stages before QGP thermalization ($\tau < \tau_0$) was mostly inferred by utilizing data from the low-$p_\perp$ sector [20–22] ($p_\perp \lesssim 5$ GeV). However, since high-$p_\perp$ partons effectively probe QGP properties, which in turn depend on initial stages, the idea of utilizing high-$p_\perp$ theory and data in exploring the initial stages emerged. This idea acquired an additional boost, since a wealth of precision high-$p_\perp$ R_{AA} [7–12] and v_2 [15–19] data have recently become available. Thus, the main goal of this paper is to assess to what extent and through what observables the initial stages of QGP evolution can be restrained by exploiting the energy loss of high-$p_\perp$ particles in the evolving medium.

While clarifying these issues is clearly intriguing, the results of current theoretical studies on this subject are either inconclusive or questionable [23–25] as, e.g., the energy loss parameters are fitted to reproduce the experimentally observed high-$p_\perp$ R_{AA} data individually for different analyzed initial stages. The energy loss parametrization should, however, clearly be a property of high-$p_\perp$ parton interactions with the medium, rather than of individual temperature profiles. Consequently, to more rigorously study this issue, one needs a high control on both the energy loss and the analyzed temperature (T) profiles. To achieve this, we here use our state-of-the-art dynamical energy loss formalism, embedded in Bjorken one-dimensional (1D) medium evolution [26] (DREENA-B framework). While Bjorken 1D medium evolution is not a full bulk QGP evolution model, for this particular study it has a major advantage, as it allows one to analytically introduce different evolutions before thermalization, with the same evolution after thermalization, which therefore allows one to clearly isolate only the effects of different initial stages (which would not be possible with full hydrodynamics models).

*Corresponding author: magda@ipb.ac.rs

Consequently, we will here consider the effects on high-$p_\perp$ R_{AA} and v_2 predictions of four common initial-stage cases [23], which have the same T profiles after thermalization, but differ in T profiles before the thermalization.

Furthermore, we recently demonstrated that the DREENA-B framework [27] is able to accurately reproduce both high-$p_\perp$ R_{AA} and v_2 data for diverse colliding systems and energies (Pb + Pb at 2.76 and 5.02 TeV and Xe + Xe at 5.44 TeV), for both light and heavy flavors ($h^\pm$, B, D) and all available centralities, without introducing new phenomena [28,29]. This is distinct from many other formalisms, which employ more advanced medium evolution models, but contain simplified energy loss models, which have a tendency to underestimate v_2 relative to the experimental data; this is widely known as the v_2 puzzle [30,31]. Moreover, we recently obtained that going from 1D Bjorken to full 3+1D hydrodynamics evolution [32] does not significantly change the agreement between our predictions and experimental data, strongly suggesting that, for high-$p_\perp$ data, accurate energy loss description is more important than the medium evolution. Consequently, for this study, using 1D Bjorken evolution has a major advantage of tight control over the temperature profiles used to mimic different initial states, while, at the same time, providing a reasonably realistic description of the data within our model.

The paper is organized as follows. In Sec. II, theoretical and computational frameworks are outlined. In Sec. III, we first assess the sensitivity of R_{AA} and v_2 to the aforementioned initial stages. We then adopt the approach of fitting initial temperature (T_0) to reproduce the same R_{AA} in all cases, and then assess the effect of thus obtained "modified" temperature profiles on R_{AA} and v_2. We finally reexamine the validity of the widely used procedure [23–25] of fitting the energy loss parameters for different initial-stage cases to reproduce the same R_{AA}. For all these studies, we analytically pinpoint the origin of the obtained results. Our conclusions are presented in Sec. IV.

II. THEORETICAL AND COMPUTATIONAL FRAMEWORKS

To obtain the medium modified distribution of high-$p_\perp$ light and heavy flavor particles, the generic pQCD convolution formula [33,34] is utilized:

$$\frac{E_f d^3\sigma}{dp_f^3} = \frac{E_i d^3\sigma(Q)}{dp_i^3} \otimes P(E_i \to E_f) \otimes D(Q \to H_Q), \quad (1)$$

where indexes f and i refer to the final hadron (H_Q) and initial parton (Q), respectively. $\frac{E_i d^3\sigma(Q)}{dp_i^3}$ denotes the parton initial momentum distribution, calculated according to [35]. $P(E_i \to E_f)$ represents the energy loss probability based on our dynamical energy loss formalism (see below). $D(Q \to H_Q)$ stands for the fragmentation function of a parton into a hadron (H_Q), where for the light hadrons and D and B mesons we apply fragmentation functions of de Florian, Sassot, and Stratmann (DSS) [36], Braaten, Cheung, Fleming, and Yuan (BCFY) [37], and Kartvelishvili, Likhoded, and Petrov (KLP) [38], respectively.

The dynamical energy loss formalism [39–41] includes several unique features in modeling jet-medium interactions, whereby we previously showed [42] that all the ingredients are important for accurately describing experimental data: (1) The finite size QCD medium, that consists of dynamical (moving) as opposed to static scattering centers, which allows longitudinal momentum exchange with the medium constituents. (2) The calculations are done within the finite temperature generalized hard-thermal-loop approach [43], so that infrared divergences are naturally regulated in a highly nontrivial manner, contrary to many models which apply tree-level (vacuumlike) propagators [44–47]. (3) Both radiative [40,41] and collisional [39] contributions are calculated within the same theoretical framework. (4) The generalizations to a finite magnetic mass [48], running coupling [33], and beyond the soft-gluon approximation [49] are performed. In this paper, for the magnetic to electric mass ratio we assume the value $\mu_M/\mu_E = 0.5$, since various nonperturbative [50,51] approaches reported it to be in the range 0.4–0.6. (5) The energy loss probability comprises also multigluon [52] and path-length [34] fluctuations. The path-length fluctuations are calculated according to the procedure presented in [53], and are provided in Ref. [54].

As outlined in Ref. [27], the analytical expression for a single gluon radiation spectrum, in an evolving medium, reads

$$\frac{dN_{rad}}{dx\,d\tau} = \frac{C_2(G)C_R}{\pi} \frac{1}{x} \int \frac{d^2\mathbf{q}}{\pi} \frac{d^2\mathbf{k}}{\pi} \frac{\mu_E^2(T) - \mu_M^2(T)}{[\mathbf{q}^2 + \mu_E^2(T)][\mathbf{q}^2 + \mu_M^2(T)]} T\alpha_s(ET)\alpha_s\left(\frac{\mathbf{k}^2 + \chi(T)}{x}\right)$$

$$\times \left[1 - \cos\left(\frac{(\mathbf{k} + \mathbf{q})^2 + \chi(T)}{xE^+}\tau\right)\right] \frac{2(\mathbf{k} + \mathbf{q})}{(\mathbf{k} + \mathbf{q})^2 + \chi(T)} \left[\frac{\mathbf{k} + \mathbf{q}}{(\mathbf{k} + \mathbf{q})^2 + \chi(T)} - \frac{\mathbf{k}}{\mathbf{k}^2 + \chi(T)}\right], \quad (2)$$

where $\mathbf{k}$ and $\mathbf{q}$ denote transverse momenta of radiated and exchanged gluons, respectively, $C_2(G) = 3$, $C_R = 4/3$ ($C_R = 3$) for the quark (gluon) jet, while $\mu_E(T)$ and $\mu_M(T)$ are electric (Debye) and magnetic screening masses, respectively. Temperature dependent Debye mass [55] is obtained by self-consistently solving Eq. (5) from Ref. [27]. α_s is the (temperature dependent) running coupling [56], E is the initial jet energy, while $\chi(T) = M^2 x^2 + m_g^2(T)$, where x is the longitudinal momentum fraction of the jet carried away by the emitted gluon, M is the mass of the quark ($M_{u,d,s} \approx \mu_E(T)/\sqrt{6}$, i.e., the thermal mass, whereas $M_c = 1.2$ GeV and $M_b = 4.75$ GeV) or gluon jet, and $m_g(T) = \mu_E(T)/\sqrt{2}$ [57] is the effective gluon mass in finite temperature QCD medium. Note that for all parameters we use standard literature values, i.e., we do not include additional fitting parameters when comparing our predictions with experimental data.

The analytical expression for the collisional energy loss per unit length in the evolving medium is given by [27]

$$\frac{dE_{\text{coll}}}{d\tau} = \frac{2C_R}{\pi v^2} \alpha_s(ET)\alpha_s\big(\mu_E^2(T)\big) \int_0^\infty n_{\text{eq}}(|\vec{\mathbf{k}}|, T)d|\vec{\mathbf{k}}| \left[\int_0^{|\vec{\mathbf{k}}|/(1+v)} d|\vec{\mathbf{q}}| \int_{-v|\vec{\mathbf{q}}|}^{v|\vec{\mathbf{q}}|} \omega d\omega + \int_{|\vec{\mathbf{k}}|/(1+v)}^{|\vec{\mathbf{q}}|_{\text{max}}} d|\vec{\mathbf{q}}| \int_{|\vec{\mathbf{q}}|-2|\vec{\mathbf{k}}|}^{v|\vec{\mathbf{q}}|} \omega d\omega \right]$$

$$\times \left[|\Delta_L(q, T)|^2 \frac{(2|\vec{\mathbf{k}}| + \omega)^2 - |\vec{\mathbf{q}}|^2}{2} + |\Delta_T(q, T)|^2 \frac{(|\vec{\mathbf{q}}|^2 - \omega^2)[(2|\vec{\mathbf{k}}| + \omega)^2 + |\vec{\mathbf{q}}|^2]}{4|\vec{\mathbf{q}}|^4}(v^2|\vec{\mathbf{q}}|^2 - \omega^2) \right], \tag{3}$$

where $n_{\text{eq}}(|\vec{\mathbf{k}}|, T) = \frac{N}{e^{|\vec{\mathbf{k}}|/T} - 1} + \frac{N_f}{e^{|\vec{\mathbf{k}}|/T} + 1}$ is the equilibrium momentum distribution [58] comprising gluons, quarks, and antiquarks ($N = 3$ and $N_f = 3$ are the numbers of colors and flavors, respectively). k is the four-momentum of the incoming medium parton, v is velocity of the initial jet, and $q = (\omega, \vec{\mathbf{q}})$ is the four-momentum of the exchanged gluon. $|\vec{\mathbf{q}}|_{\text{max}}$ is provided in Ref. [39], while $\Delta_T(T)$ and $\Delta_L(T)$ are effective transverse and longitudinal gluon propagators given by Eqs. (3) and (4) in Ref. [27].

One of the assets of our energy loss formalism is the fact that energy loss explicitly depends on T, which makes it naturally suited for examining the QGP properties via implementation of various temperature profiles. In this paper, the temperature dependence on proper time (τ) is taken according to the ideal hydrodynamical 1D Bjorken expansion [26] $T(\tau) \sim \sqrt[3]{(\tau_0/\tau)}$, with thermalization time $\tau_0 = 0.6$ fm [59,60]. The initial QGP temperature T_0 for the chosen centrality bin is not a free parameter, i.e., it is constrained starting from the ALICE effective temperature [61] and following the numerical procedure outlined in Ref. [62]. In this paper, we will concentrate on mid-central 30–40% centrality region at 5.02 TeV Pb + Pb at the LHC, which corresponds to $T_0 = 391$ MeV [27]. However, we performed an extensive study on all centrality regions (as in [27]), and checked that the results and conclusions obtained here are the same irrespectively of the centrality region (results not shown for brevity). The QGP transition temperature is considered to be $T_C \approx 160$ MeV [63].

The DREENA-B framework is applied to generate predictions for two main high-$p_\perp$ observables: R_{AA} and v_2. R_{AA} is defined as the ratio of the quenched $A + A$ spectrum to the $p + p$ spectrum, scaled by the number of binary collisions N_{bin}:

$$R_{\text{AA}}(p_T) = \frac{dN_{\text{AA}}/dp_T}{N_{\text{bin}}dN_{pp}/dp_T}; \tag{4}$$

while for intuitive understanding of the underlying effects we also use [54]

$$R_{\text{AA}} \approx \frac{R_{\text{AA}}^{\text{in}} + R_{\text{AA}}^{\text{out}}}{2}, \tag{5}$$

where $R_{\text{AA}}^{\text{in}}$ and $R_{\text{AA}}^{\text{out}}$ denote in-plane and out-of-plane nuclear modification factors, respectively. The expression for the high-$p_\perp$ elliptic flow is derived in [23] (see also [54,64,65]), under the assumption of negligible higher harmonics at high $p_\perp \gtrsim 10$ GeV, leading to

$$v_2 \approx \frac{1}{2} \frac{R_{\text{AA}}^{\text{in}} - R_{\text{AA}}^{\text{out}}}{R_{\text{AA}}^{\text{in}} + R_{\text{AA}}^{\text{out}}}. \tag{6}$$

The advantage of using Eq. (6) for high-$p_\perp$ predictions is that it is computationally significantly less demanding than the commonly used v_2 expression (see, e.g., Eq. (1) from [15]). However, to explicitly verify its applicability, we checked that, for average temperature profiles, Eq. (6) will lead to the same result (up to less than 1% difference) as the commonly used azimuthally dependent expression.

We also note that the approach to experimentally infer v_2 (see, e.g., Eq. (16) in [15]) is different from the above-mentioned theoretical approaches. However, that approach could lead to different v_2 predictions only if event-by-event fluctuations are considered (which we do not do in this study). We also note that the importance of event-by-event fluctuations in adequately addressing high-$p_\perp$ v_2 is currently an open question; i.e., in [30], it was proposed that event-by-event fluctuations may increase the high-$p_\perp$ v_2, while this was not supported by two subsequent independent studies [29,66].

III. RESULTS AND DISCUSSION

In the first part of this section we address how different initial stages (before the thermalization time τ_0) affect our predictions of high-$p_\perp$ R_{AA} and v_2. To this end, we consider the following four common cases of initial stages [23], which assume the same 1D Bjorken hydro temperature (T) profile [26] upon thermalization (for $\tau \geqslant \tau_0$), but have different T profiles before the thermalization (for $\tau < \tau_0$):

(a) $T = 0$, the so-called *free-streaming case*, which corresponds to neglecting interactions (i.e., energy loss) before the QGP thermalization.

(b) The *linear case*, corresponding to linearly increasing T with time from transition temperature ($T_C = 160$ MeV at $\tau_C = 0.25$ fm) to the initial temperature T_0.

(c) The *constant case*, $T = T_0$.

(d) The *divergent case*, corresponding to 1D Bjorken expansion from $\tau = 0$.

These initial stages are depicted in Fig. 1, and it is clear that (a)–(d) case ordering corresponds to gradually increasing prethermal interactions. Note that we use this classification (a)–(d) consistently throughout the paper to denote initial stages (for $\tau < \tau_0$), as well as for the entire evolution. Also, note that in this part of the study we will include experimental data for comparison with our predictions. However, to allow better visualization of our obtained numerical results, in the other two parts of the study we will omit the comparison with the data, as the error bars are large and the data remain the same. Intuitively, one would expect that introducing these prethermal interactions would increase the energy loss
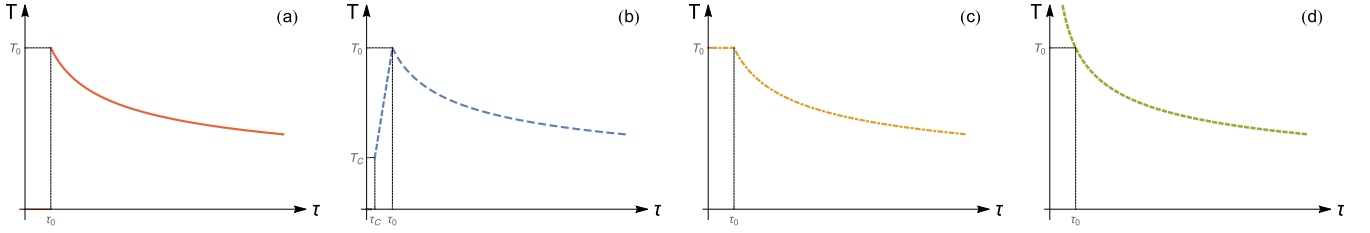
FIG. 1. Four temperature evolution profiles, which differ at the initial stages. At $\tau \geqslant \tau_0$, all profiles assume the same temperature dependence on the proper time (1D Bjorken [26]). At the initial stage, i.e., for $0 < \tau < \tau_0$, the temperature is considered to be (a) equal to zero; (b) increasing linearly from T_C to T_0 between τ_C and τ_0, otherwise zero; (c) constant and equal to T_0; and (d) a continuous function of τ matching the dependence for $\tau \geqslant \tau_0$. Note that, in each panel, T_0 has the same value at τ_0.

compared to the commonly considered free-streaming case, and consequently lead to smaller R_{AA}. In Fig. 2 we indeed observe that R_{AA} is sensitive to the initial stages for all types of particles. That is, as expected, we see that the suppression progressively increases from case (a) to case (d). However, these differences are not very large, and the current error bars at the LHC do not allow distinguishing between these scenarios, as can be seen in Fig. 2 (left).

In contrast to R_{AA}, the effect of initial stages on v_2 is intuitively less clear, as this observable nontrivially depends on the energy loss or R_{AA}'s (see Eq. (6)). From Fig. 3, we surprisingly infer that v_2 is insensitive to the presumed initial stage for all types of particles (in distinction to the results obtained in [24]), so that v_2 is unable to distinguish between different initial-stage scenarios.

To quantitatively understand this unexpected observation, in Fig. 4 we show transverse momentum dependence of R_{AA}^{in}, R_{AA}^{out}, and R_{AA} in $i = b, c, d$ cases relative to the baseline case (a) for charged hadrons. The conclusions for heavy particles are the same and therefore omitted. We distinguish three sets of curves, which correspond to the ratio of R_{AA}'s in linear (b), constant (c), and divergent (d) cases relative to the free-streaming (a) case. Note that the free-streaming case is used

as a baseline, as it corresponds to the most commonly used scenario, both in low- and high-$p_\perp$ calculations.

Each set of curves in Fig. 4 contains three lines, representing proportionality functions $\gamma(p_\perp)$, which are defined as follows:

$$\gamma_{ia}^{in} = \frac{R_{AA,i}^{in}}{R_{AA,a}^{in}}, \quad \gamma_{ia}^{out} = \frac{R_{AA,i}^{out}}{R_{AA,a}^{out}}, \quad \gamma_{ia} = \frac{R_{AA,i}}{R_{AA,a}}, \quad (7)$$

where $i = b, c, d$ denotes the corresponding cases from Fig. 1. From Fig. 4 we see that for the same i (i.e., within the same set of curves (b), (c), or (d)) the proportionality functions $\gamma_{ia}(p_\perp)$ are practically identical for the relations involving in-plane, out-of-plane, and angular averaged R_{AA}'s:

$$\gamma_{ia}^{in} \approx \gamma_{ia}^{out} \approx \gamma_{ia}. \quad (8)$$

Note also that $\gamma_{ia} < 1$, while γ_{ia}s from distinct sets significantly differ from one another (i.e., for $i \neq j \rightarrow \gamma_{ia}(p_\perp) \neq \gamma_{ja}(p_\perp)$).

Consequently, by implementing Eq. (7) in Eq. (6) and acknowledging Eq. (8), we obtain

$$v_{2,i} \approx \frac{1}{2} \frac{\gamma_{ia}(R_{AA,a}^{in} - R_{AA,a}^{out})}{\gamma_{ia}(R_{AA,a}^{in} + R_{AA,a}^{out})} = v_{2,a}, \quad (9)$$
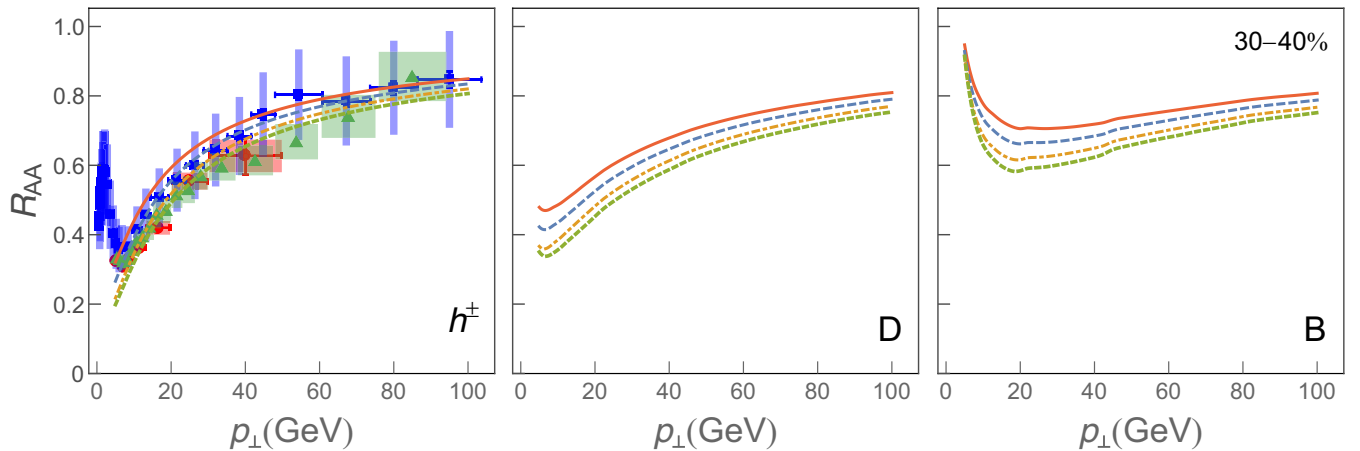

FIG. 2. R_{AA} dependence on $p_\perp$ for four different initial stages depicted in Fig. 1 is shown for charged particles (left panel), D mesons (central panel) and B mesons (right panel). For charged hadrons, the predictions are compared with 5.02 TeV Pb + Pb ALICE [7] (red circles), ATLAS [8] (green triangles), and CMS [9] (blue squares) $h^\pm$ R_{AA} experimental data. In each panel, temperature profiles from Fig. 1 are represented by a full red curve (case (a)), by a dashed blue curve (case (b)), by a dot-dashed orange curve (case (c)), and by dotted green curve (case (d)). The results correspond to the centrality bin 30–40%, and $\mu_M/\mu_E = 0.5$.
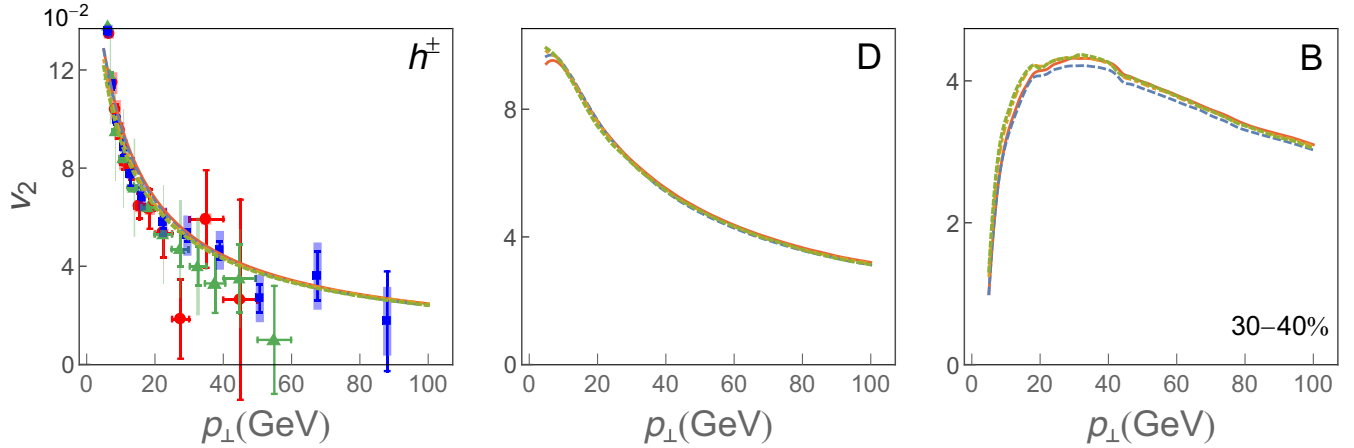
FIG. 3. v_2 dependence on $p_\perp$ for four different initial stages depicted in Fig. 1. Left, central, and right panels correspond to charged hadrons, D mesons and B mesons, respectively. For charged hadrons, the predictions are compared with 30–40% centrality 5.02 TeV Pb + Pb ALICE [15] (red circles), ATLAS [16] (green triangles), and CMS [17] (blue squares) $h^\pm$ v_2 experimental data. The labeling and remaining parameters are the same as in Fig. 2.

for any choice of $i = b, c, d$, as observed in Fig. 3. Therefore, we here showed that initial stages alone do not affect v_2, i.e., they affect only R_{AA}. R_{AA} susceptibility to the initial stages is in qualitative agreement with papers [27,67,68], where R_{AA} is shown to be only sensitive to the averaged properties of the evolving medium, i.e., average temperature ($\overline{T}$). Since R_{AA} is proportional to $\overline{T}$, and since for all four initial-stage cases (a)–(d) the $\overline{T}$ value is different ($\overline{T}_a < \overline{T}_b < \overline{T}_c < \overline{T}_d$), it is evident that R_{AA} will be different in these cases.

The fact that R_{AA} depends on the average temperature of the medium, motivates us to further explore the case in which we modify the above temperature profiles to reproduce the same average temperature. This is equivalent to reevaluating the initial temperatures for different cases from Fig. 1, and, based on the reasoning above, it is evident that new initial temperatures should satisfy the following ordering: $T_{0,d'} < T_{0,c'} < T_{0,b'} < T_{0,a'}$. This leads to T profiles, which do not differ only at early times ($\tau < \tau_0$), but represent *different evolutions altogether*. These new evolutions, that are illustrated in Fig. 5 (which is a counterpart of Fig. 1 for the second
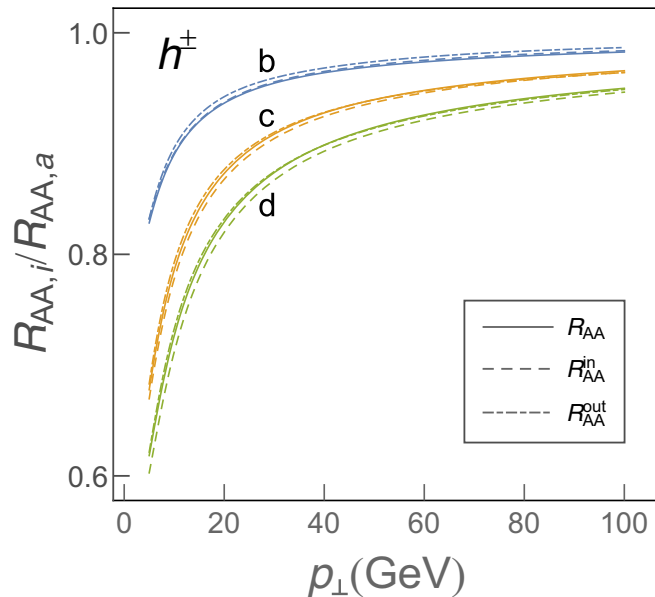

FIG. 4. Transverse momentum dependence of in-plane (dashed), out-of-plane (dot-dashed), and angular averaged (full curves) R_{AA} relative to the free-streaming (a) case for charged hadrons. Blue (upper), orange (middle), and green (lower) sets of curves correspond, respectively, to (b), (c) and (d) cases. The remaining parameters are the same as in Fig. 2.
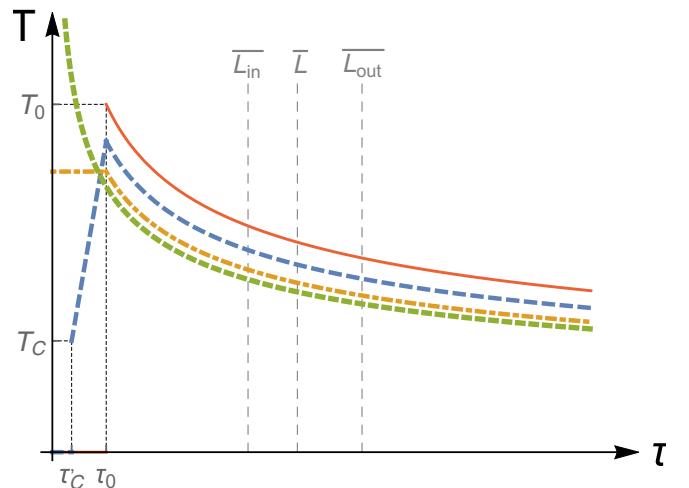
FIG. 5. Temperature dependence on the proper time in the setup with the same average temperatures. The labeling is the same as in Fig. 1, apart from the fact that initial temperatures (T_0's) now differ in these four cases. As in Fig. 1, $T_C = 160$ MeV, $\tau_0 = 0.6$ fm, and $\tau_C' = 0.27$ fm. Vertical gray dashed lines correspond to average in-medium path length ($\overline{L}$), and to the path lengths along in-plane ($\overline{L}_{in}$) and out-of-plane ($\overline{L}_{out}$) directions, as labeled in the figure.
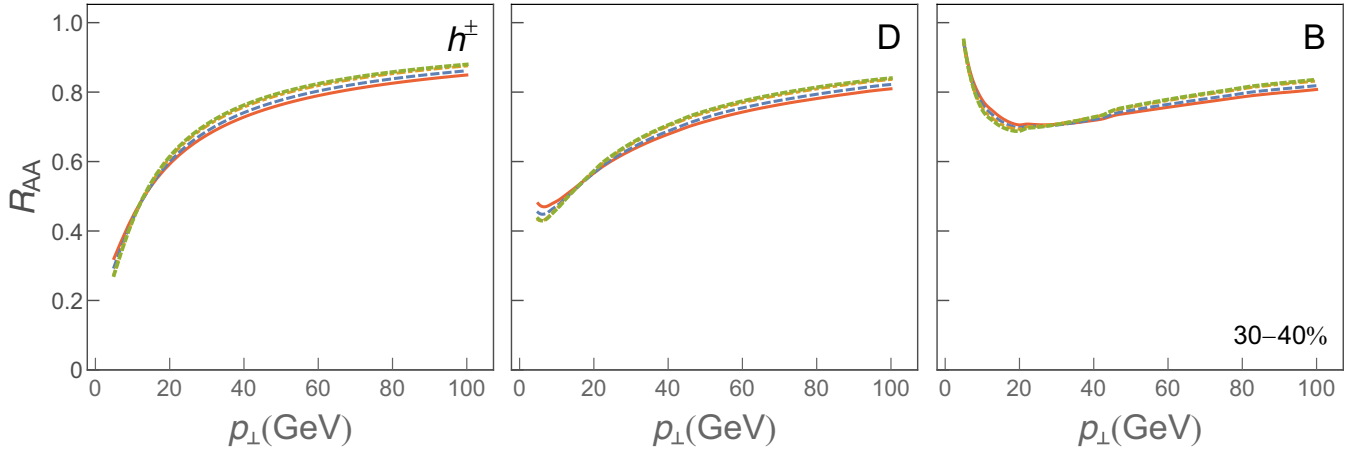
FIG. 6. R_{AA} dependence on $p_\perp$ for four different medium evolutions depicted in Fig. 5. Left, central, and right panels correspond to charged hadrons, D mesons, and B mesons, respectively. In each panel, the T profile corresponding to the case (a′) from Fig. 5 is represented by a full red curve, case (b′) by a dashed blue curve, case (c′) by a dot-dashed orange curve, and case (d′) by a dotted green curve. The results correspond to the centrality bin 30–40%, and $\mu_M/\mu_E = 0.5$.

part of this section), are denoted as (a′)–(d′) and referred to as "modified" T profiles ((a) ≡ (a′)).

In this second T-profiles setup, we first verify from Fig. 6 that R_{AA}s in all four cases practically overlap, as expected. We next address how these modified evolution cases (a′)–(d′) affect v_2. From Fig. 7 we see that v_2 is now very sensitive to the transition from the free-streaming case to other modified T profiles. More accurately, for all types of particles, the lowest v_2 is observed in the modified divergent case, while the highest v_2 is observed in the free-streaming case.

The observation from Fig. 7 leads to the following two questions: (i) Why is v_2 altered by these modified T profiles (a′)–(d′)? (ii) Are these discrepancies a consequence of different initial stages? To answer these questions, we first note that, within this setup, the differences between v_2 (observed in Fig. 7) are proportional to $R_{AA}^{in} - R_{AA}^{out}$, as the denominator in Eq. (6) (as a starting premise) remains practically unchanged (see Fig. 6). The transverse momentum dependence of $R_{AA}^{in} -$

R_{AA}^{out} is further shown in Fig. 8 for charged hadrons (as results for D and B mesons will lead to the same conclusion). We see a clear hierarchy, i.e., the largest $R_{AA}^{in} - R_{AA}^{out}$ for free streaming, descending towards the divergent case. To quantitatively understand this observation, we note that for R_{AA}^{in} the high-$p_\perp$ probes traverse, on average, the medium up to $\overline{L}_{in}$, while for R_{AA}^{out} the medium is traversed up to $\overline{L}_{out}$. Consequently, if we refer to Fig. 5, $R_{AA}^{in} - R_{AA}^{out}$ comes from the T-profile difference in the time region between $\overline{L}_{in}$ and $\overline{L}_{out}$, i.e., *upon thermalization*. Since in this region $\overline{T}_{d'} < \overline{T}_{c'} < \overline{T}_{b'} < \overline{T}_{a'}$ holds, $R_{AA}^{in} - R_{AA}^{out}$ is the largest for the free-streaming case and the smallest for the divergent case, as observed in Fig. 8, and in agreement with v_2 ordering in Fig. 7. This therefore provides clarification of why $R_{AA}^{in} - R_{AA}^{out}$, and consequently v_2, is affected by these four different QGP evolution profiles, and that this difference originates primarily from the interactions of high-$p_\perp$ partons with *thermalized QGP* and *not the initial stages*. This agrees with the first part of this section
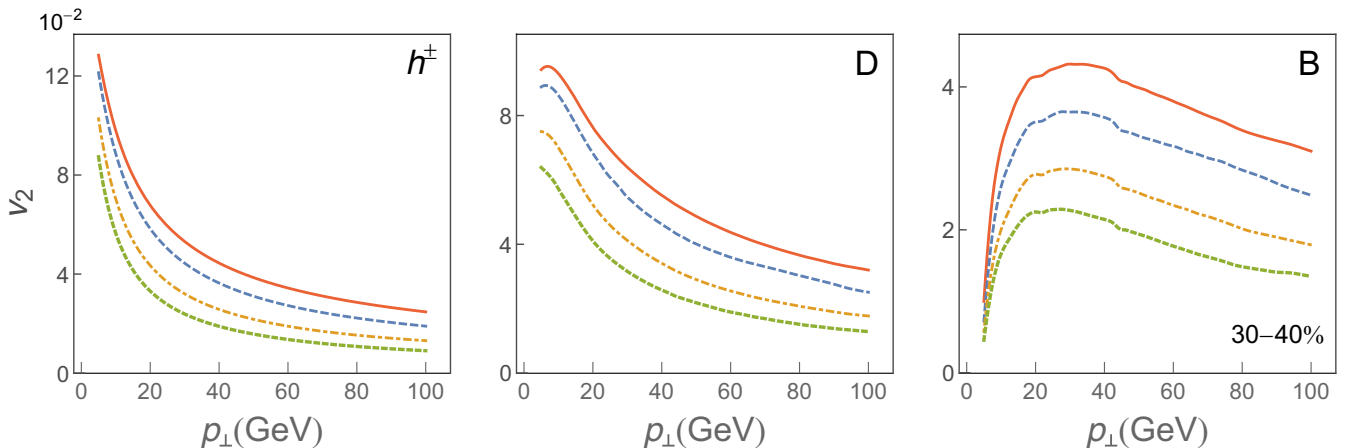

FIG. 7. v_2 dependence on $p_\perp$ for four different medium evolutions depicted in Fig. 5. Left, central, and right panels correspond to charged hadrons, D mesons, and B mesons, respectively. The labeling and remaining parameters are the same as in Fig. 6.
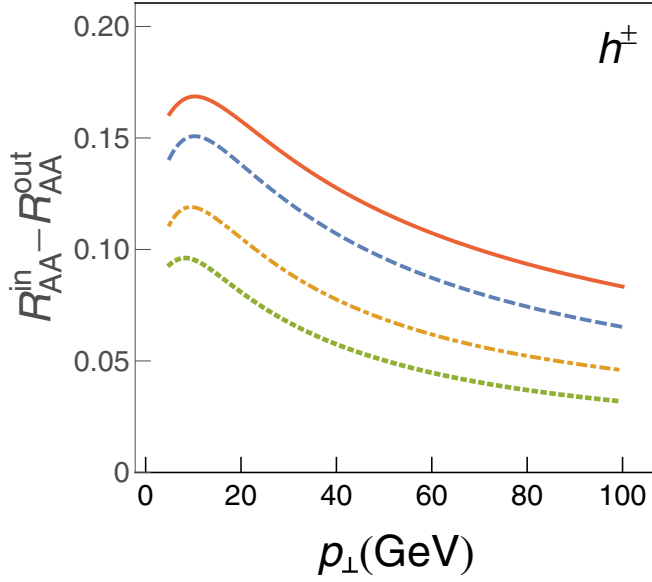
FIG. 8. $R_{\mathrm{AA}}^{\mathrm{in}} - R_{\mathrm{AA}}^{\mathrm{out}}$ dependence on $p_\perp$ for charged hadrons. The labeling and remaining parameters are the same as in Fig. 6.

TABLE I. Fitting factors values.

T profile case	C_i^{fit}
Free-streaming case (a)	1
Linear case (b)	0.87
Constant case (c)	0.74
Divergent case (d)	0.67

(Figs. 2 and 3), where we showed and explained insensitivity of v_2 to different initial stages. It is worth emphasizing that, contrary to the first part of this section, in the second part we tested the effects on R_{AA} and v_2 not from distinctive initial stages but instead from four entirely different evolutions of the QCD medium (related by the same global property, i.e., average temperature).

In the final, third part of this section we adopt a commonly used approach, in which the energy loss is fitted through change of multiplicative fitting factor in the energy loss, to reproduce the desired high-$p_\perp$ R_{AA}, e.g., the one that best fits the experimental data (see, e.g., [24,30,65,69–71]). To this end, we use the same four T profiles from the first part of this section (Fig. 1), while in our full-fledged calculations (see Sec. II) we introduce an additional multiplicative fitting factor (free parameter) C_i^{fit}, $i = b, c, d$. C_i^{fit} is then estimated for each initial-stage case as a best fit to the free-streaming R_{AA} (see Table I). Thus-obtained R_{AA}s are shown in the left panel of Fig. 9 only for the representative case of $h^\pm$, as the same conclusions stand for both light and heavy flavor hadrons. From the left panel of this figure we observe practically overlapping R_{AA}s in all (a)–(d) cases, as anticipated, which is obtained by decreasing C_i^{fit} consistently from the free-streaming to the divergent case (each $C_i^{\mathrm{fit}} \leqslant 1$) in order to *compensate* for the higher energy losses in the corresponding cases compared to the case (a).

The effect of different T profiles from Fig. 1 after introduction of multiplicative fitting factor C_i^{fit} in the full-fledged numerical procedure on v_2 is depicted in the right panel of Fig. 9, where we see that elliptic flow in (a)–(d) cases notably differs; i.e., it is the highest in the free-streaming case while it is the lowest in the divergent case. Based on this observation, one could naively infer that initial stages, i.e., the $\tau < \tau_0$ region (the only region in which T profiles differ), have a significant effect on v_2, as recently observed by an alternative approach [24].

However, this kind of reasoning is inconsistent with our analysis outlined in the first two parts of this section, as well as with intuitive expectation that introduction of the
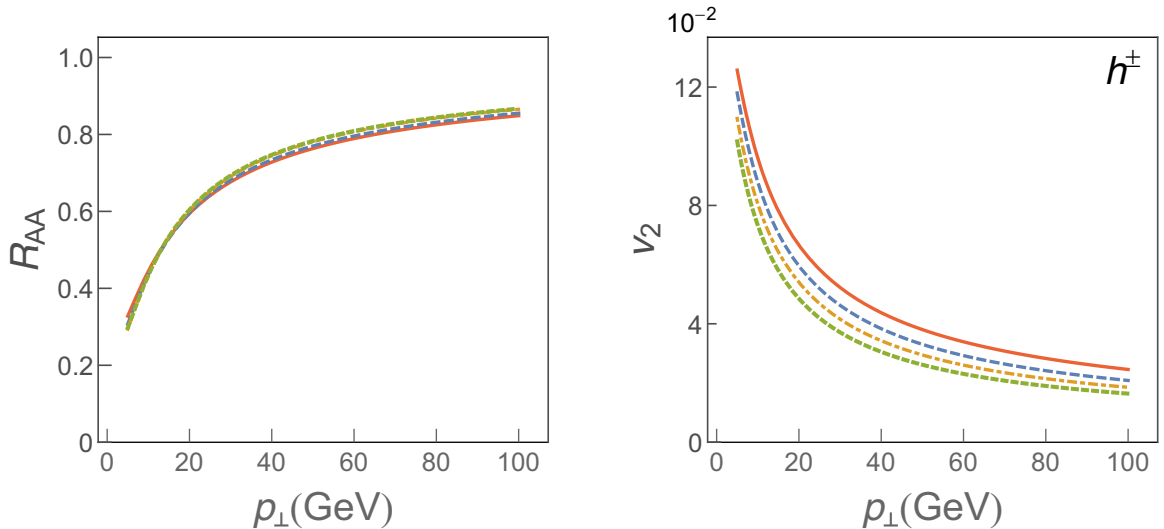

FIG. 9. R_{AA} (left panel) and v_2 (right panel) dependence on $p_\perp$ for charged hadrons, when an additional energy loss multiplicative factor is introduced to reproduce the free-streaming R_{AA}, in four different initial-stage cases depicted in Fig. 1. The labeling and remaining parameters are the same as in Fig. 2.
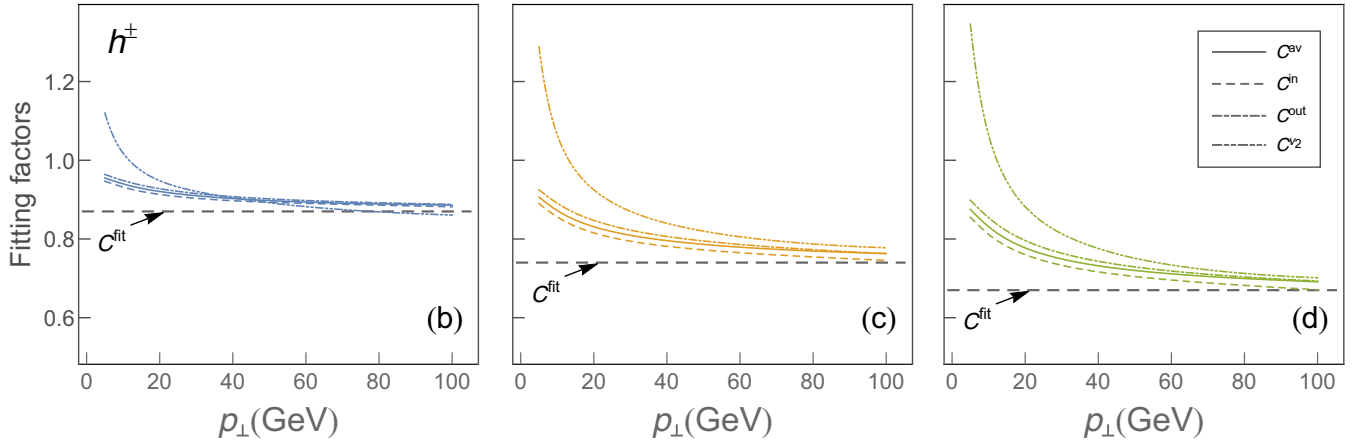
FIG. 10. Comparison of four fitting factors defined by Eq. (16) with the C_i^{fit} value, obtained from full-fledged numerical procedure, in *linear* (b) (left), *constant* (c) (central) and *divergent* (d) (right panel) cases. C factors represented by full, long-dashed, dot-dashed, and dot-dot-dashed curves correspond to $h^{\pm}$ angular averaged, in-plane, and out-of-plane R_{AA} and v_2 cases, respectively. The horizontal gray dashed line represents the energy loss fitted value C_i^{fit}. The results correspond to the centrality bin 30–40%, and $\mu_M/\mu_E = 0.5$.

energy loss at the initial stage affects R_{AA}. To quantitatively understand this result, we introduce asymptotic scaling behavior [27,54,72]. That is, for higher $p_{\perp}$ of the initial jet, and for higher centralities (where fractional energy loss is expected to be small), we can make the following estimates:

$$\Delta E/E \approx \chi \overline{T}^m \overline{L}^n, \quad R_{\text{AA}} \approx 1 - \frac{l-2}{2}\frac{\Delta E}{E} = 1 - \xi \overline{T}^m \overline{L}^n, \tag{10}$$

where m, n are proportionality factors, $\overline{T}$ is the average temperature of the QGP, $\overline{L}$ denotes the average path length traversed by the jet, χ is a proportionality factor (that depends on $p_{\perp}$ and flavor of the jet). $\xi = \frac{l-2}{2}\chi$, where l is the steepness of a power law fit to the transverse momentum distribution.

If $\Delta E/E$ is fitted by additional multiplicative factor C, the new $R_{\text{AA}}^{\text{fit}}$ becomes

$$R_{\text{AA},i}^{\text{fit}} \approx 1 - C_i \xi \overline{T}_i^m \overline{L}_i^n \approx 1 - C_i(1 - R_{\text{AA},i}), \tag{11}$$

where $i = b, c, d$ and C_i ($C_i < 1, \forall i$) denotes the fitting factor, and the last part of Eq. (11) is obtained by using Eq. (10), leading to

$$C_i \approx \frac{1 - R_{\text{AA},i}^{\text{fit}}}{1 - R_{\text{AA},i}}. \tag{12}$$

We note that Eq. (12) is applicable to the average, in-plane and out-of-plane R_{AA}s, since the same fitting factor is consistently applied in all three cases. By imposing the condition (which quantifies the equivalence of fitted R_{AA} in (b)–(d) cases to the free-streaming case)

$$R_{\text{AA},i}^{\text{fit}} = R_{\text{AA},a}, \tag{13}$$

and by applying Eqs. (5)–(8) and (13), together with Eqs. (10) and (11) and their in-plane and out-of-plane analogs, we obtain

$$v_{2,i}^{\text{fit}} \approx \frac{1}{2}\frac{C_i(R_{\text{AA},i}^{\text{in}} - R_{\text{AA},i}^{\text{out}})}{2R_{\text{AA},a}} = \frac{1}{2}\frac{C_i \gamma_{ia}(R_{\text{AA},a}^{\text{in}} - R_{\text{AA},a}^{\text{out}})}{R_{\text{AA},a}^{\text{in}} + R_{\text{AA},a}^{\text{out}}}$$
$$= C_i \gamma_{ia} v_{2,a}, \tag{14}$$

which can also be written as

$$C_i \approx \frac{v_{2,i}^{\text{fit}}}{\gamma_{ia} v_{2,a}}. \tag{15}$$

From Eq. (14), we see that decrease of v_2^{fit} in (b)–(d) cases compared to (a) is a result of a fitting factor $C_i(p_{\perp})$ (which is smaller than 1), as well as the proportionality function $\gamma_i(p_{\perp})$ (also smaller than 1). However, note that Eq. (14) describes asymptotic behavior at very high $p_{\perp}$, where, as shown earlier, γs approach 1. Consequently, the diminishing of elliptic flow compared to the case (a) is predominantly due to a decrease of the *artificially imposed fitting factor C*. Therefore, we obtain that, contrary to [24], *initial stages are not* mainly responsible for the obtained differences (the right panel of Fig. 9) in the v_2^{fit} curves for different T profiles. Moreover, this argument, as well as the obtained inconsistency of the results in this and the first two parts of the paper, implies that application of multiple fitting procedure for each different initial stage may result in incorrect energy loss estimates and in misinterpreting the underlying physics.

To asses if this qualitative conclusion indeed holds, i.e., that v_2 susceptibility observed in Fig. 9 (as well as in [24]) is indeed mainly a consequence of a fitting factor in the energy loss, in Fig. 10 we check the consistency of Eqs. (12) and (15) with the full-fledged numerical calculations. That is, a nontrivial consequence of Eqs. (12) and (15) is that C_i factors for the average, in-plane, and out-of-plane R_{AA}'s (Eq. (12)) and v_2 (Eq. (15)), should be the same in high-$p_{\perp}$ limit, and moreover overlap with C_i^{fit} in this limit. To this end, we define the C factors (originating from Eqs. (12) and (15))

$$C_i^{\text{in}} = \frac{1 - R_{\text{AA},i}^{\text{in,fit}}}{1 - R_{\text{AA},i}^{\text{in}}}, \quad C_i^{\text{out}} = \frac{1 - R_{\text{AA},i}^{\text{out,fit}}}{1 - R_{\text{AA},i}^{\text{out}}},$$

$$C_i^{av} = \frac{1 - R_{\text{AA},i}^{\text{fit}}}{1 - R_{\text{AA},i}}, \quad C_i^{v_2} = \frac{1}{\gamma_{ia}}\frac{v_{2,i}^{\text{fit}}}{v_{2,a}} \tag{16}$$

and compare them with C_i^{fit}, for each separate initial-stages case, $i = b, c, d$. Note that, while terms themselves on the right-hand side of each expression in Eq. (16) are obtained from Eqs. (12) and (15) in the high-$p_\perp$ limit (and consequently are expected to overlap in this limit, if our analytical estimate is valid), we calculate C_i^{fit}, and the terms on the right-hand side of each expression in Eq. (16), through full-fledged numerical procedure. We indeed observe that, for each i and at high-$p_\perp$, C_i^{in}, C_i^{out}, C_i^{av}, and $C_i^{v_2}$ factors are practically overlapping, and approach the value C_i^{fit}. Consequently, this highly nontrivial observation confirms that our qualitative conclusion is valid, and that v_2 susceptibility in this case is indeed mainly a consequence of an additionally introduced fitting factor.

IV. CONCLUSIONS

Traditionally, the features of initial stages before QGP thermalization are explored through comparison of bulk medium simulations and low-$p_\perp$ data. On the other hand, the recent abundance of high-$p_\perp$ experimental data motivates exploiting the high-$p_\perp$ energy loss in studying the initial stages. We here utilized state-of-the-art dynamical energy loss embedded in analytical 1D Bjorken medium expansion (DREENA-B framework), which allowed us to tightly control the analyzed temperature profiles. In particular, we considered four temperature profiles, which are identical after thermalization but are different before thermalization, corresponding to four commonly considered initial-stage cases. This allowed us to study the effects of different initial-stage cases on high-$p_\perp$ R_{AA} and v_2 predictions, under highly controlled conditions, by combining full-fledged numerical results and analytical estimates used to interpret the experimental results.

We found that high-$p_\perp$ R_{AA} is sensitive to the prethermalized stages of the medium evolution; however, within the current error bars, the sensitivity is not sufficient to distinguish between different scenarios. On the other hand, the high-$p_\perp$ v_2 is unexpectedly insensitive to the initial stages. We furthermore found that previously reported sensitivity [24] of high-$p_\perp$ v_2 to initial stages is mainly a consequence of the fitting procedure in which the parameters in the energy loss are adjusted to reproduce experimentally observed R_{AA} individually for different initial-stage cases. On the other hand, if the same global property, in particular the same average temperature, is imposed to tested temperature profiles, high sensitivity of high-$p_\perp$ v_2 is again obtained. This sensitivity is, however, a consequence of differences in final rather than initial stages. Overall, our results underscore that the simultaneous study of high-$p_\perp$ R_{AA} and v_2, with consistent that is, fixed energy loss parameters across the entire study and controlled temperature profiles (reflecting only the differences in the initial stages), is crucial to impose accurate constraints on the initial stages.

ACKNOWLEDGMENTS

[1] J. C. Collins and M. J. Perry, Phys. Rev. Lett. **34**, 1353 (1975).

[2] G. Baym and S. A. Chin, Phys. Lett. B **62**, 241 (1976).

[3] M. Gyulassy and L. McLerran, Nucl. Phys. A **750**, 30 (2005).

[4] E. V. Shuryak, Nucl. Phys. A **750**, 64 (2005); Rev. Mod. Phys. **89**, 035001 (2017).

[5] B. Jacak and P. Steinberg, Phys. Today **63**(5), 39 (2010).

[6] B. Muller, J. Schukraft, and B. Wyslouch, Annu. Rev. Nucl. Part. Sci. **62**, 361 (2012).

[7] S. Acharya *et al.* (ALICE Collaboration), J. High Energy Phys. 11 (2018) 013.

[8] ATLAS Collaboration, Report No. ATLAS-CONF-2017-012 (unpublished).

[9] V. Khachatryan *et al.* (CMS Collaboration), J. High Energy Phys. 04 (2017) 039.

[10] S. Jaelani (ALICE Collaboration), Int. J. Mod. Phys. Conf. Ser. **46**, 1860018 (2018).

[11] J. Wang (CMS Collaboration), Nucl. Part. Phys. Proc. **289–290**, 249 (2017).

[12] T. W. Wang (CMS Collaboration), Nucl. Part. Phys. Proc. **289–290**, 229 (2017).

[13] A. Adare *et al.* (PHENIX Collaboration), Phys. Rev. Lett. **101**, 232301 (2008); Phys. Rev. C **87**, 034911 (2013).

[14] B. I. Abelev *et al.* (STAR Collaboration), Phys. Lett. B **655**, 104 (2007).

[15] S. Acharya *et al.* (ALICE Collaboration), J. High Energy Phys. 07 (2018) 103.

[16] M. Aaboud *et al.* (ATLAS Collaboration), Eur. Phys. J. C **78**, 997 (2018).

[17] A. M. Sirunyan *et al.* (CMS Collaboration), Phys. Lett. B **776**, 195 (2018).

[18] S. Acharya *et al.* (ALICE Collaboration), Phys. Rev. Lett. **120**, 102301 (2018).

[19] A. M. Sirunyan *et al.* (CMS Collaboration), Phys. Rev. Lett. **120**, 202301 (2018).

[20] F. Gelis and B. Schenke, Annu. Rev. Nucl. Part. Sci. **66**, 73 (2016).

[21] G. Aad *et al.* (ATLAS Collaboration), J. High Energy Phys. 11 (2013) 183.

[22] H. Niemi, G. S. Denicol, H. Holopainen, and P. Huovinen, Phys. Rev. C **87**, 054901 (2013).

[23] J. Xu, A. Buzzatti, and M. Gyulassy, J. High Energy Phys. 08 (2014) 063.

[24] C. Andres, N. Armesto, H. Niemi, R. Paatelainen, and C. A. Salgado, Phys. Lett. B **803**, 135318 (2020).

[25] R. Katz, C. A. G. Prado, J. Noronha-Hostler, J. Noronha, and A. A. P. Suaide, arXiv:1906.10768.

[26] J. D. Bjorken, Phys. Rev. D **27**, 140 (1983).

[27] D. Zigic, I. Salom, M. Djordjevic, and M. Djordjevic, Phys. Lett. B **791**, 236 (2019).

[28] J. Xu, J. Liao, and M. Gyulassy, Chin. Phys. Lett. **32**, 092501 (2015).

[29] S. Shi, J. Liao, and M. Gyulassy, Chin. Phys. C **42**, 104104 (2018); **43**, 044101 (2019).

[30] J. Noronha-Hostler, B. Betz, J. Noronha, and M. Gyulassy, Phys. Rev. Lett. **116**, 252301 (2016).

[31] S. K. Das, F. Scardina, S. Plumari, and V. Greco, Phys. Lett. B **747**, 260 (2015).

[32] M. Djordjevic *et al.* (unpublished).

[33] M. Djordjevic and M. Djordjevic, Phys. Lett. B **734**, 286 (2014).

[34] S. Wicks, W. Horowitz, M. Djordjevic, and M. Gyulassy, Nucl. Phys. A **784**, 426 (2007).

[35] Z. B. Kang, I. Vitev, and H. Xing, Phys. Lett. B **718**, 482 (2012); R. Sharma, I. Vitev, and B. W. Zhang, Phys. Rev. C **80**, 054902 (2009).

[36] D. de Florian, R. Sassot, and M. Stratmann, Phys. Rev. D **75**, 114010 (2007).

[37] M. Cacciari and P. Nason, J. High Energy Phys. 09 (2003) 006; E. Braaten, K.-M. Cheung, S. Fleming, and T. C. Yuan, Phys. Rev. D **51**, 4819 (1995).

[38] V. G. Kartvelishvili, A. K. Likhoded, and V. A. Petrov, Phys. Lett. B **78**, 615 (1978).

[39] M. Djordjevic, Phys. Rev. C **74**, 064907 (2006).

[40] M. Djordjevic, Phys. Rev. C **80**, 064909 (2009).

[41] M. Djordjevic and U. Heinz, Phys. Rev. Lett. **101**, 022302 (2008).

[42] B. Blagojevic and M. Djordjevic, J. Phys. G **42**, 075105 (2015).

[43] J. I. Kapusta, *Finite-Temperature Field Theory* (Cambridge University Press, Cambridge, 1989).

[44] R. Baier, Y. L. Dokshitzer, A. H. Mueller, S. Peigne, and D. Schiff, Nucl. Phys. B **483**, 291 (1997); R. Baier, Yu. L. Dokshitzer, A. H. Mueller, S. Peigne, and D. Schiff, **484**, 265 (1997).

[45] N. Armesto, C. A. Salgado, and U. A. Wiedemann, Phys. Rev. D **69**, 114003 (2004).

[46] M. Gyulassy, P. Levai, and I. Vitev, Nucl. Phys. B **594**, 371 (2001).

[47] X. N. Wang and X. F. Guo, Nucl. Phys. A **696**, 788 (2001).

[48] M. Djordjevic, Phys. Lett. B **709**, 229 (2012).

[49] B. Blagojevic, M. Djordjevic, and M. Djordjevic, Phys. Rev. C **99**, 024901 (2019).

[50] Y. Maezawa, S. Aoki, S. Ejiri, T. Hatsuda, N. Ishii, K. Kanaya, N. Ukita, and T. Umeda (WHOT-QCD Collaboration), Phys. Rev. D **81**, 091501(R) (2010).

[51] A. Nakamura, T. Saito, and S. Sakai, Phys. Rev. D **69**, 014506 (2004).

[52] M. Gyulassy, P. Levai, and I. Vitev, Phys. Lett. B **538**, 282 (2002).

[53] A. Dainese, Eur. Phys. J. C **33**, 495 (2004).

[54] D. Zigic, I. Salom, J. Auvinen, M. Djordjevic, and M. Djordjevic, J. Phys. G **46**, 085101 (2019).

[55] A. Peshier, arXiv:hep-ph/0601119.

[56] R. Field, *Applications of Perturbative QCD* (Perseus Books, Cambridge, MA, 1995).

[57] M. Djordjevic and M. Gyulassy, Phys. Rev. C **68**, 034914 (2003).

[58] E. Braaten and M. H. Thoma, Phys. Rev. D **44**, 1298 (1991).

[59] P. F. Kolb and U. W. Heinz, in *Quark-Gluon Plasma 3*, edited by R. C. Hwa and X.-N. Wang (World Scientific, Singapore, 2004), p. 634.

[60] J. E. Bernhard, J. S. Moreland, and S. A. Bass, Nucl. Phys. A **967**, 293 (2017).

[61] M. Wilde (ALICE Collaboration), Nucl. Phys. A **904–905**, 573c (2013).

[62] M. Djordjevic, M. Gyulassy, R. Vogt, and S. Wicks, Phys. Lett. B **632**, 81 (2006).

[63] A. Bazavov *et al.* (HotQCD Collaboration), Phys. Rev. D **90**, 094503 (2014).

[64] P. Christiansen, K. Tywoniuk, and V. Vislavicius, Phys. Rev. C **89**, 034912 (2014).

[65] B. Betz and M. Gyulassy, J. High Energy Phys. 08 (2014) 090 [Erratum: 10 (2014) 043].

[66] S. Cao, L. G. Pang, T. Luo, Y. He, G. Y. Qin, and X. N. Wang, Nucl. Part. Phys. Proc. **289–290**, 217 (2017).

[67] T. Renk, Phys. Rev. C **85**, 044903 (2012).

[68] D. Molnar and D. Sun, Nucl. Phys. A **932**, 140 (2014); **910–911**, 486 (2013).

[69] J. Noronha-Hostler, B. Betz, M. Gyulassy, M. Luzum, J. Noronha, I. Portillo, and C. Ratti, Phys. Rev. C **95**, 044901 (2017).

[70] C. A. G. Prado, J. Noronha-Hostler, R. Katz, A. A. P. Suaide, J. Noronha, and M. G. Munhoz, Phys. Rev. C **96**, 064903 (2017).

[71] S. Cao *et al.* (JETSCAPE Collaboration), Phys. Rev. C **96**, 024909 (2017).

[72] M. Djordjevic, D. Zigic, M. Djordjevic, and J. Auvinen, Phys. Rev. C **99**, 061902(R) (2019).